Monthly Notices of the ROYAL ASTRONOMICAL SOCIETY

MNRAS **505,** 1153–1161 (2021) https://doi.org/10.1093/mnras/stab1262
Advance Access publication 2021 May 4

Constraints on the sub-pc environment of the nearby Type Iax SN 2014dt from deep X-ray and radio observations

C. M. Stauffer [1]★ R. Margutti,[1] J. D. Linford,[2] L. Chomiuk,[3] D. L. Coppejans,[1] L. Demarchi,[1] W. Jacobson-Galán,[1] J. Bright [1] R. J. Foley,[4] A. Horesh[5] and A. Baldeschi[1]

[1]*Center for Interdisciplinary Exploration and Research in Astrophysics (CIERA) and Department of Physics and Astronomy, Northwestern University, Evanston, IL 60208, USA*
[2]*National Radio Astronomy Observatory New Mexico Array Operations Center,1003 Lopezville Rd, Socorro, NM 87801, USA*
[3]*Department of Physics and Astronomy, Michigan State University, 567 Wilson Road, East Lansing, MI 48824, USA*
[4]*Department of Astronomy and Astrophysics, University of California, Santa Cruz, CA 95064, USA*
[5]*Racah Institute of Physics, The Hebrew University of Jerusalem, Jerusalem 91904, Israel*

Accepted 2021 April 30. Received 2021 April 29; in original form 2021 March 22

ABSTRACT

We present X-ray and radio observations of what may be the closest Type Iax supernova (SN) to date, SN 2014dt (d = 12.3–19.3 Mpc), and provide tight constraints on the radio and X-ray emission. We infer a specific radio luminosity $L_R < (1.0–2.4) \times 10^{25}$ erg s^{-1} Hz^{-1} at a frequency of 7.5 GHz and a X-ray luminosity $L_X < 1.4 \times 10^{38}$ erg s^{-1} (0.3–10 keV) at ∼38–48 d post-explosion. We interpret these limits in the context of Inverse Compton (IC) emission and synchrotron emission from a population of electrons accelerated at the forward shock of the explosion in a power-law distribution $N_e(\gamma_e) \propto \gamma_e^{-p}$ with p = 3. Our analysis constrains the progenitor system mass-loss rate to be $\dot{M} < 5.0 \times 10^{-6} M_\odot$ yr^{-1} at distances $r \lesssim 10^{16}$ cm for an assumed wind velocity $v_w = 100$ km s^{-1}, and a fraction of post-shock energy into magnetic fields and relativistic electrons of $\epsilon_B = 0.01$ and $\epsilon_e = 0.1$, respectively. This result rules out some of the parameter space of symbiotic giant star companions, and it is consistent with the low mass-loss rates expected from He-star companions. Our calculations also show that the improved sensitivity of the next-generation Very Large Array (ngVLA) is needed to probe the very low-density media characteristic of He stars that are the leading model for binary stellar companions of white dwarfs giving origin to Type Iax SNe.

Key words: supernovae – SN2014dt, transients: supernovae.

1 INTRODUCTION

Type Iax supernovae (SNe) are a peculiar class of thermonuclear explosions. After the first member was identified in 2002 (Li et al. 2003), dozens of members of the Type Iax supernova class have since been discovered (Foley et al. 2013). Observationally, Type Iax SNe show clear spectroscopic similarities with Type Ia SNe at maximum light (Li et al. 2003; Branch et al. 2005; Chornock et al. 2006; Phillips et al. 2007; Foley et al. 2009a, b), which suggests a physical connection to thermonuclear explosions of C/O (or C/O/Ne) white dwarfs (WDs) in binary systems (see Jha 2017 for a recent review). However, a key physical difference with respect to Type Ia SNe is that SNe Iax may not always completely destroy the WD progenitor star, but may instead leave behind a bound remnant (e.g. Foley et al. 2010a; Jordan et al. 2012; Kromer et al. 2013; Fink et al. 2014; Long et al. 2014), as was proposed for SN 2012Z (Foley et al. 2009b, 2016; McCully et al. 2014a). A fundamental question in the study of SNe Iax is the nature of the companion star of the primary WD. In this paper, we present deep X-ray and radio observations of one of the closest Type Iax SN to date, SN 2014dt ($d \sim$ 12.3-19.3 Mpc; Foley et al. 2015; Fox et al. 2015). These observations provide tight constraints on the density of the nearby environment of the explosion, which was sculpted by the recent mass-loss history of the companion star, enabling insight into the nature of the progenitor system.

Unlike Type Ia SNe, which show maximum light ejecta expansion velocities of $v \sim$10 000 km s^{-1}, Type Iax SNe typically have lower ejecta velocities (2000 km s^{-1} $\lesssim$ v $\lesssim$ 8000 km s^{-1}; e.g. Foley et al. 2009a, 2013; Narayan et al. 2011; McCully et al. 2014a, b; White et al. 2015), which, on average, suggests a less energetic explosion than Type Ia SNe (however Stritzinger et al. 2015 inferred an explosion kinetic energy $E_k \sim 10^{51}$ erg for SN 2012Z, similar to SNe Ia). SNe Iax also show lower peak optical luminosities corresponding to absolute V-band magnitudes in the range $-13 \gtrsim M_V \gtrsim -19$ mag, and typically have faster rise times to maximum light when compared to Type Ia SNe (McClelland et al. 2010; Magee et al. 2016, 2017; Jha 2017; Stritzinger et al. 2014a, b), which points at lower ejecta mass and ^{56}Ni mass. Additionally, the optical spectra of SNe Iax never become dominated by broad forbidden lines at late times (i.e. never become fully 'nebular', e.g. Sahu et al. 2008; McCully et al. 2014a; Yamanaka et al. 2015; Foley et al. 2016). Finally, SNe Iax show a marked preference for late-type host galaxies, suggesting a connection to a relatively young stellar population (Foley et al. 2010a; Lyman et al. 2013, 2018; Li et al. 2017; Takaro et al. 2020). Currently, only one SN Iax (SN 2008ge) has been discovered in an S0-type galaxy, with no evidence for star formation or massive stars (Foley et al. 2010a).

★ E-mail: cstauffer@u.northwestern.edu

The nature of the stellar companions to WDs that produce SNe Iax is largely unknown. The leading paradigm is that these companions are He-stars, as originally postulated by Foley et al. (2013), and supported by binary simulations (e.g. Wang, Justham & Han 2013). From an observational perspective, the notion of He-star companions is supported by the first detection of a progenitor system of a WD explosion for the Type Iax SN 2012Z, reported by McCully et al. (2014a). These authors find a luminous blue source in pre-explosion *Hubble Space Telescope* (*HST*) images at the location of SN 2012Z, which is consistent with the presence of a He-star companion.[1] Currently, SNe 2008ge, 2012Z, and 2014dt are the only SNe Iax with deep pre-explosion imaging. No progenitor system was detected for either SN 2008ge (Foley et al. 2010a) or SN 2014dt (Foley et al. 2015). For SN 2008ge *HST* images ruled out the most massive stars as progenitors with initial masses $M < 85$ M$_\odot$ for main-sequence stars and $M < 12$ M$_\odot$ for horizontal and red giant branch stars (Foley et al. 2010b).

In the specific case of SN 2014dt, the classes of stellar companions ruled out by *HST* pre-explosion imaging include the following (Foley et al. 2015): (i) main-sequence stars with initial mass $M > 16$ M$_\odot$ and (ii) red giant/horizontal branch (RG/HB) stars with $M > 8$ M$_\odot$. Foley et al. (2015) also conclude that Wolf–Rayet (WR) stars are unlikely companions due to the absence of other nearby bright stars at the location of SN 2014dt. To complement this work we study the nearby environment of SN 2014dt at radio and X-ray wavelengths, which provides an indirect probe of its progenitor system.

SN 2014dt was discovered on 2014 October 29.84 UT in the M61 galaxy (in the Virgo cluster) by Koichi Itagaki (Nakano et al. 2014) and later spectroscopically classified as a Type Iax SN on 2014 October 31.20 UT by the Asiago Transient Classification Program (Ochner et al. 2014) using criteria defined in Foley et al. (2013). The optical/near-infrared (NIR) and mid-infrared (MIR) properties of SN 2014dt have been presented by Fox et al. (2015) and Kawabata et al. (2018), while the optical properties of the host-galaxy environment have been studied by Lyman et al. (2018). In addition to the progenitor limits of Foley et al. (2015), of particular interest is the finding of a very slow spectroscopic and photometric evolution of SN 2014dt at $t \geq 100$ d post-maximum (Kawabata et al. 2018) and the presence of an MIR excess of emission (Fox et al. 2015; Foley et al. 2016). In analogy with the Type Iax SN 2005hk (Foley et al. 2013), this slow evolution can be interpreted as evidence for the presence of a persistent photospheric component possibly formed within the wind launched by the surviving bound remnant WD (Kawabata et al. 2018). The optical-NIR luminosity decline of SN 2014dt is the slowest observed in well-studied SNe Iax (Kawabata et al. 2018).

In this paper, we utilize deep X-ray and radio observations of the nearby Type Iax SN 2014dt in the first ∼50 d since explosion. X-ray and radio emission originate from particles accelerated at the SN shock to relativistic speeds (e.g. Chevalier & Fransson 2006), as the blastwave plows through the circumstellar medium (CSM), which was sculpted by mass lost to the surroundings by the SN progenitor system. X-ray and radio observations of SNe from WD binary systems thus carry direct information about the mass-loss history of their stellar companions, and therefore their nature. This technique has been recently employed by Immler, Wilson & Terashima (2002), Margutti et al. (2012), Chomiuk et al. (2012), Horesh et al. (2012), Russell & Immler (2012), and Chomiuk et al. (2015). No Type Iax SN has ever been detected either in the radio or X-ray regime. From the most recent compilation by Chomiuk et al. (2015), typical radio luminosity limits are $L_{\nu,R} \lesssim 1.81 \times 10^{25}$ erg s^{-1}Hz^{-1} (at $\nu \sim 5.9$–8.4 GHz). Typical X-ray limits are $L_x \lesssim 10^{39}$ erg s^{-1} (this work). Our analysis of SN 2014dt extends the range of investigated radio and X-ray luminosities to $L_{\nu,R} \sim (1.0–2.4) \times 10^{25}$ erg s^{-1}Hz^{-1} and $L_x \sim 10^{38}$ erg s^{-1}.

This paper is organized as follows. We present the X-ray and radio observations of SN 2014dt in Section 2. We model the X-ray and radio observations in the context of IC and synchrotron emission, respectively, in Section 3 and Section 4. We discuss our constraints on the progenitor systems of Type Iax SNe and thermonuclear explosions and present our conclusions and prospects for future X-ray and radio studies of Type Iax SN in Section 5. Throughout the paper uncertainties are provided at the 68 per cent confidence level (c.l.) and upper limits at the 3σ c.l. (Gaussian equivalent) unless explicitly stated otherwise.

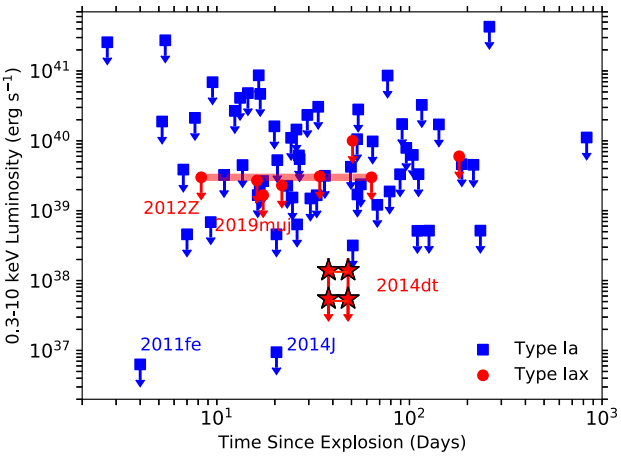

Figure 1. CXO observations of SN 2014dt (red stars) provide the deepest constraints on the X-ray luminosity of a Type-Iax SN to date. The four red stars indicate the limits derived for SN 2014dt taking the range of distance and explosion dates (MJD = 56930–56940) into account. We also plot the X-ray limits of Type-Iax SNe 2012Z and 2019muj from *Swift*-XRT observations. Red (blue) points: X-ray limits from previous observations of Type Iax (Type Ia) SNe from Russell & Immler (2012), Margutti et al. (2012), Margutti et al. (2014), and this work.

Table 1. VLA observations of SN 2014dt on 2014 November 7, corresponding to $\delta t = 28$–38 d since explosion. For each observation we provide the range of luminosity density that corresponds to the range of distances 12.3–19.3 Mpc.

Central Freq. (GHz)	Bandwidth (GHz)	rms (mJy/beam)	L_ν (erg s^{-1} Hz^{-1})
4.8	2	0.033	$<(1.8–4.4) \times 10^{25}$
7.5	2	0.018	$<(1.0–2.4) \times 10^{25}$
20.0	4	0.019	$<(1.0–2.6) \times 10^{25}$
24.0	4	0.020	$<(1.1–2.7) \times 10^{25}$

2 OBSERVATIONS

The precise distance of M61 and the precise explosion date of SN 2014dt are unknown. Foley et al. (2015) favour the distance of 12.3 Mpc (EPM method, Bose & Kumar 2014). However, Fox et al.

[1]He-star companion is the favoured explanation but an accretion disc around a WD is also a viable interpretation. While the *HST* data alone are consistent with a massive star as well, the combination with other data makes this scenario no longer viable (McCully et al. 2014a).

Table 2. Limits on the environment density (for an ISM-like CSM) and progenitor mass-loss rate of the pre-explosion (for a wind-like CSM) derived from the radio observations of Table 1 and the modelling of Section 4. We present our inferences for the environment properties of SN 2014dt using explosion parameters derived based on the modelling of the optical bolometric light curve of SN 2014dt by Kawabata et al. (2018) (M_{ej} =(0.06–0.25) M_{ch}, E_k =(0.07–0.42)×10^{50}erg) as well as explosion parameters that are typical of Iax SNe (M_{ej} = 0.4 M_{ch}, E_k = 10^{50}erg) or to allow a direct comparison to the limits presented in Chomiuk et al. (2015). For the mass-loss rate limits we adopt v_w = 100 km s^{-1}.

CSM type	Typical SN Iax		SN 2014dt	
	$\epsilon_B = 0.1$	$\epsilon_B = 0.01$	$\epsilon_B = 0.1$	$\epsilon_B = 0.01$
n (cm^{-3}) <	4.3×10^3	2.5×10^4	1.7×10^4	1.0×10^5
$\dot{M}$ ($M_\odot yr^{-1}$) <	7.0×10^{-7}	2.8×10^{-6}	1.3×10^{-6}	5.0×10^{-6}

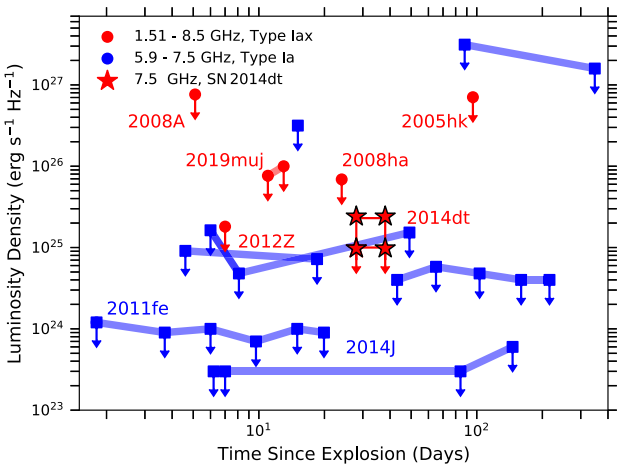

Figure 2. Radio observations of SN 2014dt (red stars) in the context of Type Ia SNe (blue) and Type Iax SNe (red) from Chomiuk et al. (2015). Four red stars limit the region of the parameter space of SN 2014dt depending on the assumed distance, explosion epoch, and taking explosion dates (MJD = 56930–56940) into account. Together with SN 2012Z (Chomiuk et al. 2015), radio observations of SN 2014dt provide the deepest constraints on radio emission from a Type Iax SN at $t > 10$ d. The radio limit on SN 2019muj is from Perez-Torres et al. (2019).

(2015) adopt the distance of 19.3 Mpc (Photospheric magnitude method, Rodríguez, Clocchiatti & Hamuy 2014). SN 2014dt was discovered around peak optical brightness, so the explosion date is not well constrained. The time of maximum luminosity in the *B* band was constrained to 2014 October 20 (MJD ∼ 56950) (Fox et al. 2015; Foley et al. 2016; Kawabata et al. 2018; Singh et al. 2018). In the following text, we conservatively derive and discuss our results for the entire range of distances: d = 12.3–19.3 Mpc, and explosion epochs in the range between 2014 September 30 and 2014 October 10 (MJD ∼ 56930–56940) (corresponding to a rise time between 10 and 20 d, in line with other Type Iax SNe, e.g. Magee et al. 2016, 2017; Jha 2017).

2.1 X-ray Observations with the CXO

We initiated deep X-ray observations of SN 2014dt with the Chandra X-ray Observatory (CXO) on 2014 November 17 under an approved DDT program 15508486 (PI Margutti), corresponding to 38–48 d since explosion. The data have been reduced with the CIAO software package (version 4.11), with calibration data base CALDB version 4.8.2. Standard ACIS data filtering has been applied. The total exposure time of our observations is 19.8 ks. No X-ray source is detected at the SN position. Assuming pure Poisson statistics we infer a 3σ upper limit of 2.5×10^{-4} c s^{-1} in the 0.5–8 keV energy band, which implies an absorbed flux limit of $F_x < 3.5 \times 10^{-15}$erg s^{-1} cm^{-2} (0.3–10 keV) for a $F_\nu \propto \nu^{-1}$ non-thermal spectrum (which applies to both synchrotron and IC emission). The Galactic neutral hydrogen (NH) column density in the direction of SN 2014dt is exceptionally low where NH =$1.7 \times 10^{20}$$cm^{-2}$ (Kalberla et al. 2005) allowing the use of Chandra low-energy passband down to 0.3 keV. The corresponding 0.3–10 keV luminosity limit for d = 12.3–19.3 Mpc is $L_x < (0.6 - 2.0) \times 10^{38}$ erg s^{-1} (Fig. 1). The presence of diffuse soft X-ray emission from the host galaxy prevents us from reaching deeper limits.

2.2 Radio observations with the VLA

Deep radio observations were acquired with the Karl G. Jansky Very Large Array (VLA) with program VLA/14A-494 (PI A. Horesh) on 2014 November 7. The observations were taken at *C*, *X*, and *K* bands. These data were calibrated using the CASA pipeline version 1.3.1 (McMullin et al. 2007). We inspected the calibrated data and performed additional flagging in AIPS (Greisen 2003). To minimize frequency-dependent artefacts in imaging, we split each of the *C* and *K* bands in two and imaged each half separately, producing four images centred at 4.8, 7.4, 20.0, and 24.0 GHz. We used `difmap` for imaging (Shepherd 1997).

Diffuse emission from the host galaxy dominates the images at 4.8 and 7.5 GHz. To improve our sensitivity to point sources at these frequencies, we removed all baselines shorter than 0.01 Mλ. The host galaxy flux does not contribute significantly to the 20 and 24 GHz images. All baselines were used to create images at these frequencies. SN 2014dt is not detected at any frequency. We report the off-source root mean squared (rms) measurements for the images using natural weighting in Table 2. We compare the 3σ 7.5 GHz radio luminosity limits calculated for SN 2014dt to a sample of Type-Ia SNe and Iax SNe from Chomiuk et al. (2015) in Fig. 2. Together with SN 2012Z, our radio limits on SN 2014dt sample the lowest radio luminosities of Type-Iax SNe.

3 CONSTRAINTS ON THE ENVIRONMENT DENSITY FROM X-RAY OBSERVATIONS

X-ray emission generated by the upscattering of seed optical photospheric photons by a population of relativistic electrons accelerated at the SN shock (IC radiation) dominates the early ($t \lesssim 40$ d) X-ray luminosity from SNe that explode in low-density media (like Type Ia or Type Ib/c SNe, e.g. Chevalier & Fransson 2006). We independently verified this statement using the synchrotron modelling detailed in Section 4 and found that the expected luminosity of synchrotron emission in the X-rays at these times is negligible

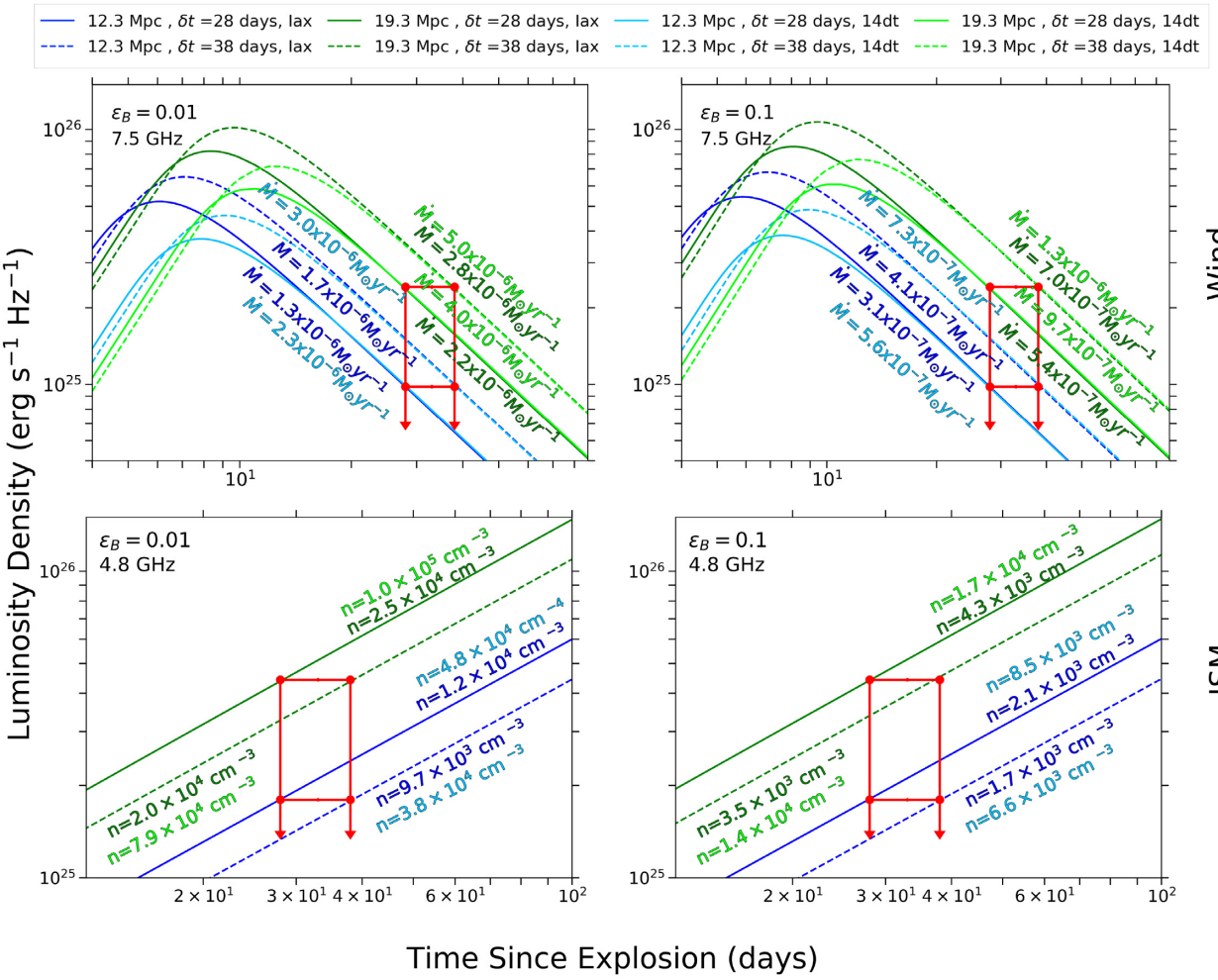

Figure 3. Temporal evolution of the radio emission from a blast wave plowing through an ISM-like CSM for 4.8 GHz (lower panels) or wind-like CSM for 7.5 GHz (upper panels). Our calculations assume $\epsilon_e = 0.1$ and $\epsilon_B = 0.1$ (right-hand panels) or $\epsilon_B = 0.01$ (left-hand panels), and adopt the wind velocity $v_w = 100\,\mathrm{km\,s^{-1}}$ to calculate $\dot{M}$. In dark shades of blue and green we show the radio luminosity for a 'typical' Type Iax SN explosion parameters where $M_{ej} = 0.4\,\mathrm{M_{ch}}$ and $E_k = 10^{50}$ erg. Lighter shades of blue and green represent the model for the lower E_k and M_{ej} values inferred for SN 2014dt at the range of explosion dates MJD = 56930–56940, which are $M_{\rm ej} = (0.06\text{–}0.25)\,\mathrm{M_{ch}}$ and $E_{\rm k} = (0.07\text{–}0.42) \times 10^{50}$ erg (Kawabata et al. 2018).

compared to the observed emission. We therefore continue under the assumption that at the time of our CXO observations of SN 2014dt, IC dominates. After the SN optical peak, the IC emission became progressively fainter with time as the optical emission of the SN faded, and non-thermal synchrotron emission became the dominant X-ray component.

We adopt the IC formalism of Margutti et al. (2012, 2014). The IC emission depends on the explosion parameters (i.e. ejecta mass M_{ej} and kinetic energy E_k), the outer density profile of the ejecta $\rho_{SN} \propto R^{-n}$, the environment density profile $\rho_{CSM} \propto r^{-s}$, the energy spectrum of the accelerated electrons $N_e(\gamma) \propto \gamma^{-p}$, the fraction of post-shock energy into relativistic electrons ϵ_e, and the SN bolometric luminosity $L_{\rm bol}$. We assume $n \sim 10$ as appropriate for compact stellar progenitors (Matzner & McKee 1999; Chevalier & Fransson 2006), we employ a wind-density profile $s = 2$ and we use $p = 3$, as typically inferred from radio observations of SNe (e.g. Soderberg et al. 2006c, b, a, 2010), where the IC luminosity is $L_{\rm IC}(t) \propto L_{\rm bol}(t)$. We use the optical bolometric luminosity curve of SN 2014dt derived by Kawabata et al. (2018).

We present the results of our IC modelling for two choices of the explosion parameters (Fig. 3). First we assume the parameters inferred by Kawabata et al. (2018) from the modelling of the post-peak optical/NIR light curve of SN 2014dt. Kawabata et al. (2018) derive $M_{\rm ej} = 0.06\text{–}0.25\,\mathrm{M_{ch}}$ (with $\mathrm{M_{ch}} = 1.4\,\mathrm{M_\odot}$) and $E_{\rm k} = (0.07\text{–}0.42) \times 10^{50}$ erg. The low ejecta mass and kinetic energy are consistent with a surviving remnant scenario. For these parameters we find $\dot{M} < 3.5 \times 10^{-1}\,\mathrm{M_\odot yr^{-1}}$ for $v_w = 100\,\mathrm{km\,s^{-1}}$. Second, we provide a calculation of the mass-loss limit assuming the typical explosion parameters of Type Iax SNe as a class, i.e. $M_{ej} \sim 0.4\,\mathrm{M_{ch}}$ and $E_k \sim 10^{50}$ erg. For these parameters we infer $\dot{M} < 1.1 \times 10^{-1}\,\mathrm{M_\odot yr^{-1}}$ for $v_w = 100\,\mathrm{km\,s^{-1}}$. In the first scenario the inferred mass-loss limits are slightly less constraining as there is less ejecta mass carrying energy to power the emission (Fig. 4).

4 CONSTRAINTS ON THE ENVIRONMENT DENSITY FROM RADIO OBSERVATIONS

In stellar explosions the thermal optical emission traces the slow-moving ejecta ($v \leq 10\,000\,\mathrm{km\,s^{-1}}$) to which the bulk of the kinetic energy is coupled, while radio observations probe the fastest ejecta ($v \geq 0.1c$). The radio emission originates from the interaction of the

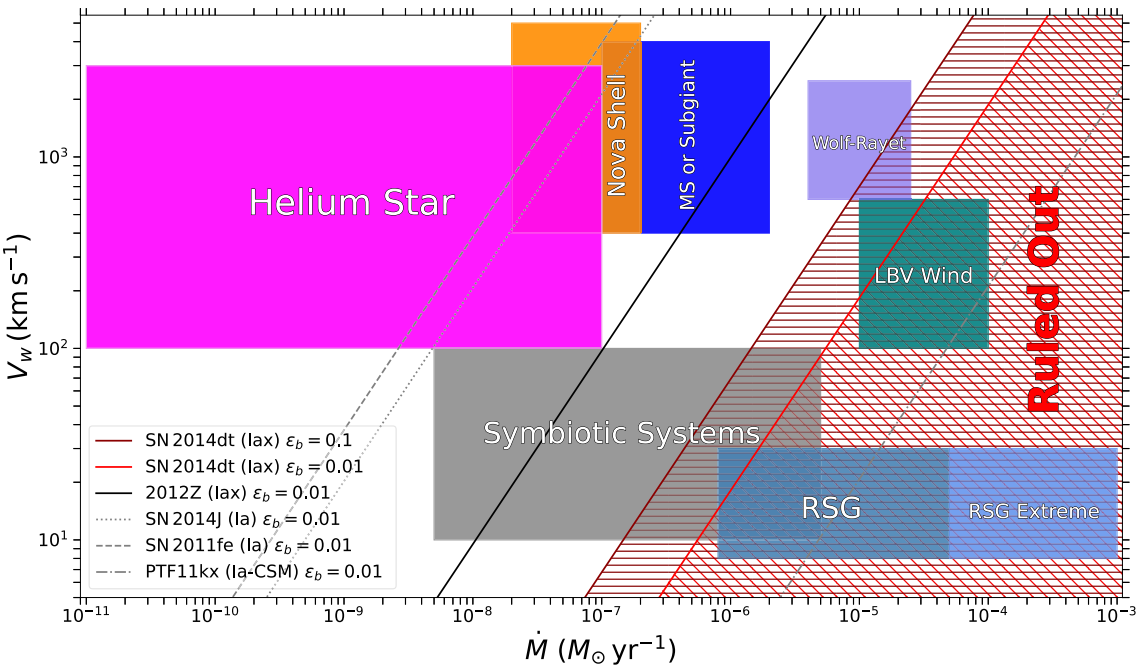

Figure 4. Constraints on the parameter space of the mass-loss rate from the binary progenitor system $\dot{M}$ and velocity of the progenitor wind v_w. The hatched regions indicate the part of the parameter space that is ruled out. For SN 2014dt we derive the most conservative $\dot{M}$ for $\epsilon_B = 0.01$ and $\epsilon_B = 0.1$ as $\dot{M} < 5.0 \times 10^{-6} \mathrm{M}_\odot\ \mathrm{yr}^{-1} (\mathrm{v_w}/100\,\mathrm{km\,s^{-1}})$ and $\dot{M} < 1.3 \times 10^{-6} \mathrm{M}_\odot\ \mathrm{yr}^{-1} (\mathrm{v_w}/100\,\mathrm{km\,s^{-1}})$, respectively. We compare these limits to those for $\epsilon_\mathrm{B} = 0.01$ of SNe Iax 2012Z (Chomiuk et al. 2015) and 2019muj (derived in Appendix A using the radio upper limits from Perez-Torres et al. 2019), and SNe Ia 2014J (Chomiuk et al. 2014), 2011fe (Chomiuk et al. 2012), and the Type Ia-CSM PTF11kx (Dilday et al. 2012; Chomiuk et al. 2015) where $\epsilon_\mathrm{B} = 0.01$. Using the observed mass-loss rates and wind velocities in massive stars from Chomiuk et al. (2012) and Terreran et al. (2019), we find that a portion of the parameter space associated with giant star (GS) companions and Wolf-Rayet (WR) stars is ruled out for $\epsilon_\mathrm{b} = 0.1$ for SN 2014dt. For both values of ϵ_B we can rule out Red Super Giant Stars (RSG) and most of the Luminous Blue Variable (LBV) stars wind-like CSM parameter space. We do not constrain the parameter space of He-stars, Nova-like shells, or MS stars.

fastest SN ejecta with the local environment that results from the recent mass-loss from the progenitor star.

The observed synchrotron radiation depends on (i) the explosion parameters (M_{ej}, E_k), (ii) on the density of the surrounding medium ($\rho_{CSM} \propto r^{-s}$ with $s = 2$ for a wind profile and $s = 0$ for an interstellar medium ISM-like CSM profile), (iii) on the fraction of post-shock energy into magnetic fields and relativistic electrons (ϵ_B and ϵ_e, respectively), and (iv) on the electron distribution $N_e(\gamma) \propto \gamma^{-p}$. We adopt the formalism of Chomiuk et al. (2015) for $p = 3$ and infer a density of the environment assuming both ISM and wind-like environments. Our results are reported in Table 2 . As before we estimate the density and mass-loss rate limits both for the explosion parameters of SN 2014dt and for typical SN Iax explosion parameters to allow a direct comparison to the results presented by Chomiuk et al. (2015).

5 DISCUSSION AND CONCLUSIONS

We have presented a sensitive search for X-ray and radio emission (Figs 1 and 2) from the very nearby Type Iax SN 2014dt. Because of the presence of diffuse X-ray emission from the host galaxy, we found that the X-ray limits were not as constraining as the radio limits, and we therefore focus our discussion on the results from the radio modelling of Section 2.2.

Radio observations of SN 2014dt allowed us to place tight constraints on the environment density of a Type Iax SN. For the progenitor system of SN 2014dt we find that the most conservative $\dot{M}$ limits for $\epsilon_B = 0.01$ and $\epsilon_B = 0.1$ are $\dot{M} < 5.0 \times 10^{-6} M_\odot\ yr^{-1} (v_w/100\,\mathrm{km\,s^{-1}})$ and $\dot{M} < 1.3 \times 10^{-6} M_\odot\ yr^{-1} (v_w/100\,\mathrm{km\,s^{-1}})$, respectively. For standard assumptions on the SN ejecta profile and shock dynamics of Chomiuk et al. (2015), the forward shock radius for a wind-stratified CSM environment is

$$R_{FS} = (5.0 \times 10^{15}\mathrm{cm})\, M_{\mathrm{ej,\,Ch}}^{-0.32}\, E_{k,\,51}^{0.44}\, A_*^{-0.12}\, t_{10}^{0.88}, \quad (1)$$

where t_{10} is the time since explosion normalized to 10 d, $A_* = (A/5 \times 10^{11})\mathrm{g\,cm^{-1}}$ where $A_* = 1$ corresponds to $\dot{\mathrm{M}}/\mathrm{v_w} = 10^{-6} \frac{\mathrm{M}_\odot\,\mathrm{yr}^{-1}}{100\,\mathrm{km\,s^{-1}}}$ (Chevalier & Fransson 2006), $\mathrm{M_{ej,Ch}}$ is the ejecta mass in units of Chandrasekhar mass, and $E_{k,\,51}$ is the kinetic energy in units of 10^{51} erg. We assume solar abundance for the CSM with mean molecular weight $\mu = 1.4$ (Chomiuk et al. 2015). Based on equation (1) the mass-loss limits above imply forward shock radii $R_{FS} \gtrsim (5\text{–}9) \times 10^{15}$ cm at 28–38 d since explosion.

We put our inferences into the context of the mass-loss parameter space of potential stellar companions to WDs in a single degenerate progenitor system in Fig. 4. Our results exclude some symbiotic systems, RSG, LBV winds, and WR stars (Fig. 4). This result is consistent with the constraints placed on the progenitor of SN 2014dt using *Hubble Space Telescope* (*HST*) pre-explosion images (Foley et al. 2015). Specifically, WR stars are disfavoured by *HST* observations as WR stars typically reside in regions with high density of bright stars, whereas SN 2014dt exploded in a sparsely populated stellar region (∼100 pc from any detected sources, and more than ∼200 pc from any particularly bright source, Foley et al. 2015).

SN 2014dt showed evidence for an excess of emission at NIR-MIR wavelengths (Fox et al. 2015). Understanding the physical origin of

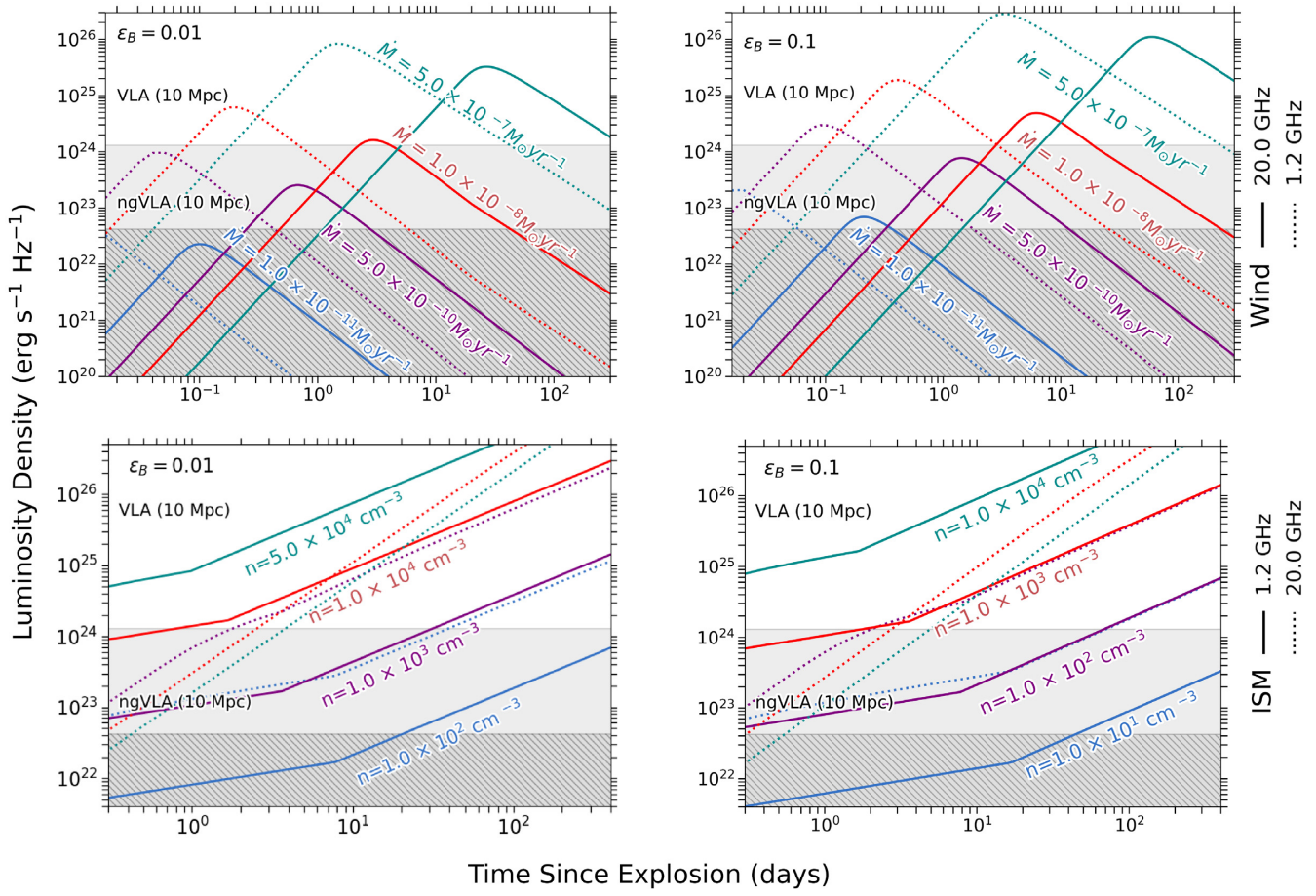

Figure 5. Radio light-curves at 1.2 GHz (thick lines) and 20 GHz (dotted lines) of Type-Iax SNe with explosion parameters similar to SN 2014dt at the range of explosion dates MJD = 56930–56940 in a wind-like (upper panels) or ISM-like (lower panels) CSM. Different colours are used for different mass-loss values (for the wind scenario) or density (for the ISM scenario). We adopt $v_w = 100\,\mathrm{km\,s^{-1}}$. The right-hand panels adopt an optimistic $\epsilon_B = 0.1$, while the left-hand panels use the fiducial value of $\epsilon_B = 0.01$ value. The black region indicates the region which can not be probed by either the VLA or ngVLA, while the light grey and white region show the typical luminosity limit (3σ) for ∼1 h of ngVLA and VLA time at $\lesssim$20 GHz (Carilli et al. 2015), respectively, for a SN at 10 Mpc. This exercise shows that even in the case of a very nearby SN, the improved sensitivity of the ngVLA is necessary to probe the very low mass-loss rates of He stars that might be the companions of WDs progenitors of Iax SNe.

this excess might offer additional clues about the progenitor system of SN 2014dt. At ∼100 d after maximum optical light, Fox et al. (2015) found that the emission from SN 2014dt begins to exhibit redder colours than the Type Iax SNe 2005hk and 2012Z, reaching a colour $(B-V) \sim 1.5$ mag at ∼300 d. An MIR excess of emission was also detected about a year after explosion, which Fox et al. (2015) attributed to $\sim 10^{-5} M_\odot$ of either optically thin newly formed dust *or* optically thin pre-existing circumstellar dust, which was estimated to be at a radius $r_{bb} \geq 3 \times 10^{15}$ cm. The latter scenario would support a single degenerate progenitor system with an inferred mass-loss rate of $< 10^{-6} M_\odot yr^{-1}$ for a wind velocity $v_w = 100\,\mathrm{km\,s^{-1}}$ (Fox et al. 2015). Our radio observations rule out the presence of the dust shell at radii smaller than $\sim 10^{16}$ cm for $\epsilon_B \geq 0.1$ but do not allow us to probe the entire parameter space associated with the dust-shell scenario.

Foley et al. (2016) found the possibility of *pre-existing* dust to be unlikely due to low reddening of SN 2014dt at early times. In addition, strong limits on narrow absorption lines in the spectra of SN 2014dt indicated a gas-poor environment (Foley et al. 2015) and spectra of SN 2014dt indicated no circumstellar interaction (Foley et al. 2016). Foley et al. (2016) also found no observational evidence for temporal evolution of the line profiles (i.e. extinction of the redshifted emission line profile, which is a telltale feature of dust formation, e.g. Smith, Foley & Filippenko 2008). There were also no clear changes of the forbidden-line shapes from +270 d and +410 d, as well as no evidence for additional reddening which makes the newly formed dust scenario unlikely. An alternative explanation of the MIR excess of emission that is consistent with the observational evidence above is that of an optically thick super-Eddington wind launched by a bound remnant that survived the explosion. This scenario is supported by observations of a long-lasting photosphere and low photospheric velocities (Foley et al. 2016; see however Kawabata et al. 2018). Our radio observations cannot probe the presence of this dense wind, since this wind was launched after explosion.

We conclude with one consideration on the future of radio studies of subluminous thermonuclear explosions. Our analysis of SN 2014dt has shown how even in the case of the most nearby Type Iax SNe, deep VLA observations acquired at relatively early times are unable to probe the parameter space of He-star progenitors. This conclusion applies to another recently discovered nearby Type-Iax SN 2019muj, as we quantitatively demonstrate in Appendix A. The significantly improved sensitivity of the next-generation Very

Large Array (ngVLA, Carilli et al. 2015) will help explore the parameter space of the very low-density media that might be typical of thermonuclear explosions down to unprecedented limits (Fig. 5).

ACKNOWLEDGEMENTS

Margutti's team is partially supported by the Heising-Simons Foundation under grant #2018-0911 (PI: Margutti). RM is grateful to KITP for hospitality during the completion of this paper. This research was supported in part by the National Science Foundation under Grant No. NSF PHY-1748958. RM acknowledges support by the National Science Foundation under Award No. AST-1909796 and AST-1944985. Raffaella Margutti is a CIFAR Azrieli Global Scholar in the Gravity & the Extreme Universe Program, 2019, and a A. P. Sloan fellow in Physics 2019. CS is grateful to the Integrated Data-Driven Discovery in Earth and Astrophysical Sciences (IDEAS) of the National Science Foundation (NSF). WJ-G is supported by the National Science Foundation Graduate Research Fellowship Program under Grant No. DGE-1842165 and the IDEAS Fellowship Program at Northwestern University. WJ-G acknowledges support through NASA grants in support of *Hubble Space Telescope* program GO-16075. AH is grateful for the support by grants from the Israel Science Foundation, the US-Israel Binational Science Foundation (BSF), and the I-CORE Program of the Planning and Budgeting Committee and the Israel Science Foundation.

The UCSC transient team is supported in part by National Science Foundation (NSF) grant AST-1518052, the Gordon & Betty Moore Foundation, the Heising-Simons Foundation, and by a fellowship from the David and Lucile Packard Foundation to RJF.

This research has made use of the XRT Data Analysis Software (XRTDAS) developed under the responsibility of the ASI Science Data Center (ASDC), Italy.

The National Radio Astronomy Observatory is a facility of the National Science Foundation operated under cooperative agreement by Associated Universities, Inc. Fundamental Research.

We thank the entire Chandra team for carrying out our DDT observations, and the Chandra X-ray Center, which is operated by the Smithsonian Astrophysical Observatory for and on behalf of the National Aeronautics Space Administration under contract NAS8-03060.

DATA AVAILABILITY

The data underlying this article are available in the article and in its online supplementary material.

REFERENCES

Barna B. et al., 2021, MNRAS, 501, 1078
Bose S., Kumar B., 2014, ApJ, 782, 98
Branch D., Baron E., Hall N., Melakayil M., Parrent J., 2005, PASP, 117, 545
Brimacombe J. et al., 2019, Astron. Telegram, 13004, 1
Carilli C. et al., 2015, preprint (arXiv:1510.06438)
Chevalier R. A., Fransson C., 2006, ApJ, 651, 381
Chomiuk L. et al., 2012, ApJ, 750, 164
Chomiuk L. et al., 2015, ApJ, 821, 1
Chomiuk L., Zauderer B. A., Margutti R., Soderberg A., 2014, Astron. Telegram, 5800, 1
Chornock R., Filippenko A. V., Branch D., Foley R. J., Jha S., Li W., 2006, PASP, 118, 722
Dilday B. et al., 2012, Science, 337, 942
Fink M. et al., 2014, MNRAS, 438, 1762
Foley R. J. et al., 2009a, AJ, 138, 376
Foley R. J., Brown P. J., Rest A., Challis P. J., Kirshner R. P., Wood-Vasey W. M., 2009b, ApJ, 708, L61
Foley R. J. et al., 2010a, AJ, 140, 1321
Foley R. J. et al., 2010b, AJ, 140, 1321
Foley R. J. et al., 2013, ApJ, 767, 57
Foley R. J., Van Dyk S. D., Jha S. W., Clubb K. I., Filippenko A. V., Mauerhan J. C., Miller A. A., Smith N., 2015, ApJ, 798, 8
Foley R. J., Jha S. W., Pan Y. C., Zheng W. K., Bildsten L., Filippenko A. V., Kasen D., 2016, MNRAS, 461, 433
Fox O. D. et al., 2015, ApJ, 816, L13
Greisen E. W., 2003, in Heck A., ed., Astrophysics and Space Science Library, Vol. 285, Information Handling in Astronomy - Historical Vistas. Springer-Verlag, Berlin, p. 109
Horesh A. et al., 2012, ApJ, 746, 21
Immler S., Wilson A. S., Terashima Y., 2002, ApJ, 573, L27
Jha S. W., 2017, Handbook of Supernovae, 1
Jordan George C. I., Perets H. B., Fisher R. T., van Rossum D. R., 2012, ApJ, 761, L23
Kalberla P. M. W., Burton W. B., Hartmann D., Arnal E. M., Bajaja E., Morras R., Pöppel W. G. L., 2005, A&A, 440, 775
Kawabata M. et al., 2018, PASJ, 70, 111
Kromer M. et al., 2013, MNRAS, 429, 2287
Li W. et al., 2003, PASP, 115, 453
Li L. et al., 2017, MNRAS, 478, 4575
Long M. et al., 2014, ApJ, 789, 103
Lyman J. D. et al., 2018, MNRAS, 473, 1359
Lyman J. D., James P. A., Perets H. B., Anderson J. P., Gal-Yam A., Mazzali P., Percival S. M., 2013, MNRAS, 434, 527
Magee M. R. et al., 2016, A&A, 589, A89
Magee M. R. et al., 2017, A&A, 601, A62
Margutti R. et al., 2012, ApJ, 751, 134
Margutti R., Parrent J., Kamble A., Soderberg A. M., Foley R. J., Milisavljevic D., Drout M. R., Kirshner R., 2014, ApJ, 790, 52
Matzner C. D., McKee C. F., 1999, ApJ, 510, 379
McClelland C. M. et al., 2010, ApJ, 720, 704
McCully C. et al., 2014a, Nature, 512, 54
McCully C. et al., 2014b, ApJ, 786, 134
McMullin J. P., Waters B., Schiebel D., Young W., Golap K., 2007, in Shaw R. A., Hill F., Bell D. J., eds, ASP Conf. Ser. Vol. 376, Astronomical Data Analysis Software and Systems XVI. Astron. Soc. Pac., San Francisco, p. 127
Nakano S. et al., 2014, Cent. Bur. Electron. Telegrams, 4011, 1
Narayan G. et al., 2011, ApJ, 731, L11
Ochner P., Tomasella L., Benetti S., Cappellaro E., Elias-Rosa N., Pastorello A., Turatto M., 2014, Cent. Bur. Electron. Telegrams, 4011, 2
Perez-Torres M. et al., 2019, Astron. Telegram, 13105, 1
Phillips M. M. et al., 2007, PASP, 119, 360
Rodríguez Ó., Clocchiatti A., Hamuy M., 2014, AJ, 148, 107
Russell B. R., Immler S., 2012, ApJ, 748, L29
Sahu D. K. et al., 2008, ApJ, 680, 580
Shepherd M. C., 1997, in Hunt G., Payne H., eds, ASP Conf. Ser. Vol. 125, Astronomical Data Analysis Software and Systems VI. Astron. Soc. Pac., San Francisco, p. 77
Singh M. et al., 2018, MNRAS, 474, 2551
Smith N., Foley R. J., Filippenko A. V., 2008, ApJ, 680, 568
Soderberg A. M. et al., 2006a, Nature, 442, 1014
Soderberg A. M. et al., 2006c, ApJ, 650, 261
Soderberg A. M. et al., 2010, Nature, 463, 513
Soderberg A. M., Nakar E., Berger E., Kulkarni S. R., 2006b, ApJ, 638, 930
Stritzinger M. et al., 2014a, A&A, 561, A146
Stritzinger M. et al., 2014b, A&A, 561, A146
Stritzinger M. D. et al., 2015, A&A, 573, A2
Takaro T. et al., 2020, MNRAS, 493, 986
Terreran G. et al., 2019, ApJ, 883, 147
Wang B., Justham S., Han Z., 2013, A&A, 559, A94
White C. J. et al., 2015, ApJ, 799, 52
Yamanaka M. et al., 2015, ApJ, 806, 191

Table A1. Sensitivity of current (VLA) and future (SKA and ngVLA) radio telescopes at representative frequencies that are relevant to Fig. 5. The rms sensitivity is provided for a 1-h on-source observation and the luminosity limits have been calculated as 3×RMS at the nominal distance of 10 Mpc.

Telescope	Central freq. (GHz)	rms (μJy beam^{-1})	Lum. density limit (erg s^{-1} Hz^{-1})
ngVLA[a]	2.4	0.38	1.4×10^{23}
	16.4	0.20	7.2×10^{22}
SKA[b]	1.4	2.0	7.2×10^{23}
	12.5	1.2	4.3×10^{23}
VLA	1.4	8.0	2.9×10^{24}
	22.0	3.7	1.3×10^{24}

Notes.[a] https://ngvla.nrao.edu/page/performance
[b] https://www.skatelescope.org

APPENDIX A: SENSITIVITY OF CURRENT (VLA) AND FUTURE (SKA AND NGVLA) RADIO TELESCOPES

APPENDIX B: INFERENCES ON THE PROGENITOR MASS-LOSS HISTORY OF THE TYPE-IAX SN2019MUJ

SN 2019muj was discovered on 2019 August 7, UT 09:36 (MJD 58702.4) by Brimacombe et al. (2019). It was classified as a Type-Iax SN at the distance of 25.8 Mpc (Perez-Torres et al. 2019). Perez-Torres et al. (2019) found no evidence of radio emission from SN 2019muj and inferred a 3σ upper limit of $F_\nu < 96$ μJy beam^{-1} and $F_\nu < 126$ μJy beam^{-1} at 5.08 and 1.51 GHz, respectively. The corresponding upper limits on the monochromatic luminosity are $L_\nu < 7.6 \times 10^{25}$ erg s^{-1} Hz^{-1} and $L_\nu < 1.0 \times 10^{26}$ erg s^{-1} Hz^{-1} at 5.08 and 1.51 GHz, respectively, for an assumed distance of 25.8 Mpc. Using these measurements Perez-Torres et al. (2019) reported upper limits on the mass-loss rate of the supernova progenitor of $\dot{M} < 6.1 \times 10^{-8}$ M$_\odot$yr^{-1} and $\dot{M} < 5.6 \times 10^{-8}$ M$_\odot$yr^{-1} (3σ c.l.) using observations at 5.08 and 1.51 GHz, respectively, for an assumed wind speed of $v_w = 100$ km s^{-1} and optically thin synchrotron emission.

Here, we adopt the revised distance to SN 2019muj calculated by Barna et al. (2021) based on the association with the host galaxy VV 525 for which a distance was calculated with the Tully–Fisher method $d = 34.1$ Mpc. We further adopt the explosion parameters $M_{ej} = 0.12\,M_{ch}$, kinetic energy $E_k = 0.04 \times 10^{51}$ erg from the modelling of the optical light curve of SN 2019muj presented by Barna et al. (2021). Applying the synchrotron formalism of Section 4 we do not confirm the inferences from Perez-Torres et al. (2019), but rather conclude that their radio limits of SN 2019muj presented by Perez-Torres et al. (2019) do not constrain the mass-loss parameter space in either the ISM or the wind-like scenarios as we show in Figs B1 and B2. Specifically, while larger density (n) values for the ISM-like CSM or, equivalently, larger $\dot{M}$ values of the wind-like CSM model would be more luminous, denser media also cause the radio emission to peak at later times. Deep radio observations of SN 2019muj acquired at later times can potentially constrain the mass-loss parameter space of this explosion.

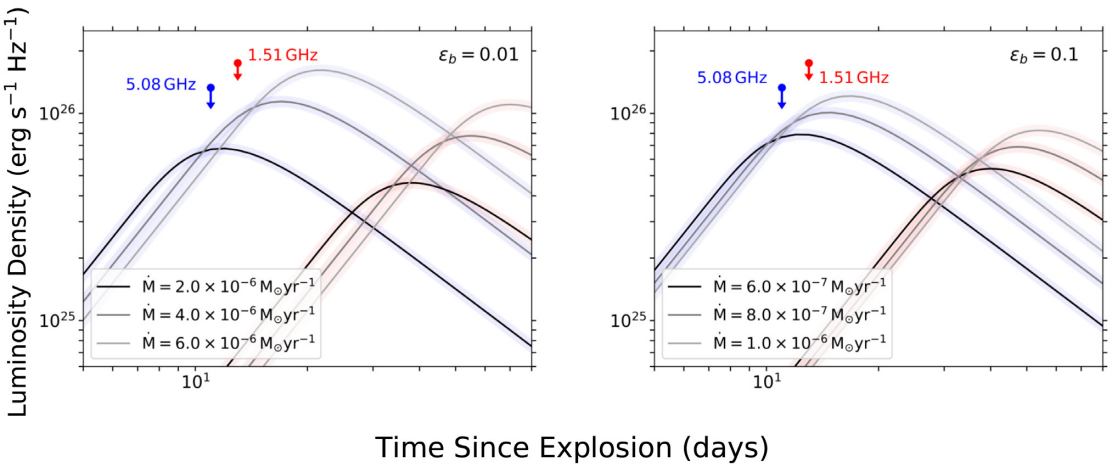

Figure B1. Temporal evolution of the specific radio luminosity powered by synchrotron emission at 1.5 GHz (brown lines) and 5.1 GHz (blue lines) for three representative $\dot{M}$ values, ϵ_B= 0.01 (left-hand panel) and $\epsilon_B = 0.1$ (right-hand panel) for SN 2019muj. We use the distance and explosion parameters inferred by Barna et al. (2021) ($d = 34$ Mpc, ejecta mass $M_{ej} = 0.12\,M_{ch}$ and kinetic energy $E_k = 0.04 \times 10^{51}$ erg), and adopt a wind velocity $v_w = 100$ km s^{-1}. Red and blue arrows: upper limit on the radio emission from SN 2019muj presented by Perez-Torres et al. (2019). The radio upper limits do not rule out any of the synchrotron models (i.e. there is no model that violates the limits, irrespective from the mass-loss rate value is), and hence do not constrain the environment properties of SN 2019muj.

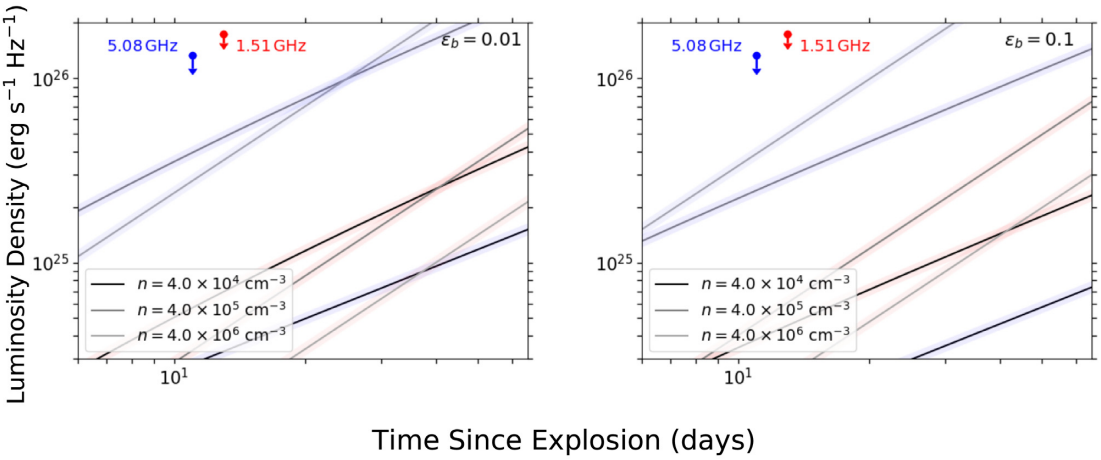

Figure B2. Same as Fig. B1 for an ISM-like CSM around SN 2019muj. Similarly to the wind-scenario, the radio upper limits do not rule out any of the synchrotron models, and hence do not constrain the environment properties of SN 2019muj.

This paper has been typeset from a TEX/LATEX file prepared by the author.